ACS APPLIED MATERIALS & INTERFACES

Research Article

www.acsami.org

Tunable Touch Sensor and Combined Sensing Platform: Toward Nanoparticle-based Electronic Skin

Meital Segev-Bar, Avigail Landman, Maayan Nir-Shapira, Gregory Shuster, and Hossam Haick*

The Department of Chemical Engineering and Russell Berrie Nanotechnology Institute, Technion, Israel Institute of Technology, Haifa 3200003, Israel

Supporting Information

ABSTRACT: In this paper, we present touch (or pressure) flexible sensors based on monolayer-capped nanoparticles (MCNPs) that are potentially inexpensive, could allow low-voltage operation, and could provide a platform for multifunctional applications. We show that modifying the mechanical and geometrical properties of the flexible substrates, on which the MCNP films are deposited, allows measuring a large span of loads ranging between tens of mg to tens of grams. All flexible sensors exhibited repeatable responses even after a large number of bending cycles. In addition, we show that modified platforms of those touch (or pressure) sensors allow precise detection and monitoring of environmental temperature and humidity. Relying on their superior characteristics, we were able to build an MCNP-based prototype allowing simultaneous detection and monitoring of multiple environmental parameters of touch (or pressure), humidity, and temperature. The excellent temperature (resolution higher than 1 °C and average error of ∼5%) and relative humidity (resolution higher than 1% RH and average error of ∼9%) sensitivities and the possibility to integrate those sensing abilities makes the suggested platform interesting for potentially inexpensive and low-voltage multifunctional *electronic-skin* applications.

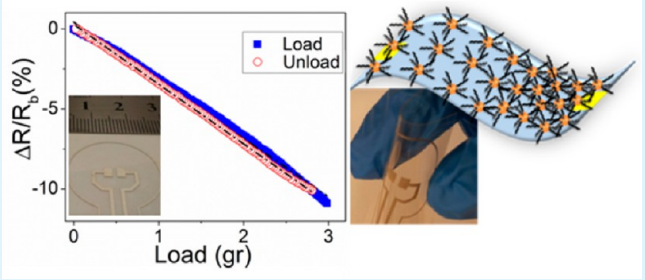

KEYWORDS: *nanoparticle, electronic skin, flexible, tunable, load sensitivity, environmental*

INTRODUCTION

Flexible sensors have attracted great interest as soft and rubbery components for various applications, such as hand-held consumer electronics and displays, as well as ultrathin health-monitoring tapes that could seamlessly be mounted onto the skin.[1,2] Inexpensive and low-power touch-sensitive platforms of flexible sensors that are based on nanowires,[3−5] carbon nanotubes,[6−9] nanoparticles,[10−12] rubber dielectric layers,[13−15] and organic field-effect transistors[16−18] have been successfully demonstrated. However, the following targets have to be met to make flexible sensors attractive for a wide range of real-world applications: (i) Development of a sensing platform that can measure a wide dynamic range of pressure, from low pressures (1−10 kPa), which would be useful for small object manipulation,[19] up to high pressures (10−100 kPa), which would be useful for lifting a person or a heavy object. (ii) Simultaneous[20−22] measuring of pressure (touch), humidity,[23] temperature and/or the presence of chemical agents.[24] (iii) Low-voltage or low-power operation (below 5 V),[25] to be compatible with commonly used batteries of portable devices today. (iv) Easier, faster, more cost-effective fabrication techniques for flexible sensors than the ones currently in use.[5,12]

Layers of monolayer-capped nanoparticles (MCNPs)[11,23,24,26−34] on flexible substrates are potential candidates for a new generation of highly sensitive flexible sensors that could meet these targets.[11,35−37] The combination of highly versatile organic monolayers with highly versatile nanocrystal (metal) cores ensures tuning the composition, functionality, and interparticle spatial properties.[27,28] Altogether, this leads to enhanced sensitivity, selectivity, detection limit, and response time, thus optimizing device performance[36,38,39] (cf., also refs 40−48 for representative real-world applications).

In theory, the electrical properties of MCNP films depend exponentially on the interparticle distance.[11] Apparently, the theoretical description of the electron transport mechanism in nanoparticle assemblies is complicated by the typical strong disorder of the MCNP arrangement, consisting of differently shaped metal clusters connected via tunnel junctions of different cross sections and gaps.[49] Nevertheless, deposition of the MCNPs on a flexible substrate allows modulating the resistance either by stretching or by bending the substrate. Geometry and mechanical properties of the substrate also affect the interparticle separation. For example, metal-enhanced fluorescence,[50] optical properties,[51] and small-angle X-ray Spectroscopy (SAXS) investigations[10] have shown that the nanoparticle separation depends on the substrate strain.

Received: February 28, 2013
Accepted: June 4, 2013
Published: June 4, 2013

Moreover, theoretical calculations have shown that the sensitivity to the tactile load of an individual sensor can be adjusted through control of the substrate's thickness.[52] Yet, for real world applications, the ability to tune the sensitivity for a large span of loads should be considered. In addition, the effects of relative humidity and temperature on flexible MCNP touch sensors and the integration of these sensing abilities have not yet been reported.

In this paper, we present MCNP-based flexible pressure sensors that are potentially inexpensive, could allow low-voltage operation, and could provide a platform for multifunctional applications. We show that these sensors allow repeatable bending or elastic deformation, with load detection limits as small as 0.2 g. The ability of these structures to measure a wide range of loads is examined by testing substrates with different geometrical and mechanical properties. In addition, we show that the same sensors can also provide highly sensitive temperature and humidity measurements. The ability to use MCNP films to measure specific physical and chemical parameters in a complex environment is demonstrated. This constitutes an important step toward the development and application of multifunctional electronic skin (e-skin).

EXPERIMENTAL SECTION

Synthesis of MCNPs. Gold(III) chloride trihydrate ($HAuCl_4 \cdot 3H_2O$), tetraoctylammonium bromide (TOAB), sodium borohydride, 3-ethoxythiophenol (ETP), decanethiol (DT), and 2-nitro-4-trifluoro-methylbenzenethiol (NTMBT) were purchased from Sigma-Aldrich. All reagents were of analytical grade and were used as received. Spherical gold nanoparticles (3−6 nm in diameter) were synthesized as described elsewhere.[32,39] Briefly, a solution of $HAuCl_4$ was added to a stirred solution of TOAB in toluene. After the solution was stirred for 10 min, the lower aqueous phase was removed. Organic ligands and sodium borohydride were subsequently added to the toluene phase. After 3 h at ice temperature, the lower aqueous phase was removed and the toluene phase was subsequently evaporated by rotary evaporation. After first washing with cold ethanol, the solution was kept at 5 °C for 18 h until achieving complete immersion. The dark brown precipitate was filtered off and washed with ethanol.

Sensor Fabrication. Electrodes were deposited on different isolating substrates (see Table 1). The electrodes were prepared using silver paste (Mouser Electronics) with an approximate thickness of a few micrometers.[53] The spacing between the adjacent electrodes was typically 1 mm in all experiments that examined the substrate effect on the load sensitivity. Mash printed electrodes by CPC Hi Technologies Ltd. with 3 mm length and variable spacing of 0.5, 1, and 3 mm were used to examine the effect of spacing between the electrodes. All of the substrates were received from DuPont (GADOT is the official distributor of DuPont special). Flexible sensors were achieved by casting 2 μL of MCNPs in solution on top of the flexible electrodes that were described above.

Table 1. Summary of the MCNP/Substrate Sensors Fabricated in the Present Study

substrate	Young's modulus (MPa)	substrate thickness (μm)	load sensitivity[a]
PVC 200[b]	2200	200	0.04 ± 0.003
Kapton 50[c]	2500	50	0.23 ± 0.03
Kapton 127	2500	127	0.04 ± 0.014
Kapton b. 131	4430	131	0.03 ± 0.008
PET 125	4200	125	0.01 ± 0.005
Mylar 36[d]	4100	36	0.31 ± 0.036
Mylar 50	4100	50	0.07 ± 0.019

[a]Load sensitivity: relative change of resistance per unit change in the load. [b]PVC: Polyvinyl chloride. [c]DuPont Kapton. [d]DuPont Mylar.

Morphology Characterization of the MCNP Films. The microstructure and morphology of the MCNP films were characterized by field emission high-resolution scanning electron microscopy (Carl Zeiss Ultra Plus FE-HRSEM). The FE-HRSEM analysis was carried out with the aid of two auxiliary means: detector of secondary electrons (SE) and detector of backscattered electrons (BSE). The SE detector provides high-resolution imaging of the surface. The BSE detector provides image contrast as a function of elemental composition as well as surface topography. The morphology of the MCNP films was additionally examined by a tapping mode atomic force microscope (AFM) (Dimension 3100 with Nanoscope IIIa controller, Veeco Instruments Inc.) that is equipped with a 100 μm × 100 μm scanner. Silicon cantilevers with a normal resonance frequency of 160 kHz and spring constants of 5 N/m (NSC14/AlBs, MikroMasch, Estonia) were used. All images were captured with a scan rate of 1−2 Hz and with a pixel resolution of 512 × 512.

Bending and Stretching Experiments. A MARK 10 ESM301 motorized test stand was used to apply strain in a constant speed of 1.5 mm/s. For *bending experiments* (Figure 1a), the stress was applied by an upper beam (downward arrow in Figure 1a) and supported by bottom beams (upward arrows in Figure 1a). Under applied stress/pressure/force, the substrate is bent. The outer (upper) surface is then subjected to compression, while the inner (lower) surface is under dilatation. The forces were measured by an Advanced Digital FORCE GAUGE, made by Mark10 USA. In these experiments, the electrical resistance was measured by A Keithley data-logger device (model 2701 DMM) controlled by a custom Labview program.

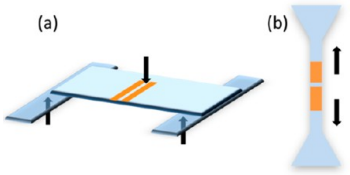

Figure 1. (a) Three-point bending setup. The points marked by the bottom arrows are the static lean beams on which the flexible substrate rests. The upper arrow is where the strain is applied. (b) Schematics for stretching setup. The substrate is in a "dog bone" shape where the grips are attached to the wider part of the sample. The arrows represent the direction of the applied strain.

In the described bending setup, the deflection δ in the point of applied load can be described as

$$\delta = \frac{PL^3}{48EI} \quad (1)$$

where P is the applied load, L is the distance between the two static beams, E is the substrates' Young modulus, and I is the moment of inertia. For rectangular shape in a bending setup this moment is defined as

$$I = \frac{bh^3}{12} \quad (2)$$

where b stands for the substrate's width and h stands for the substrate's thickness. **Note:** The values of b were similar for all substrates used in the present study.

The response of a flexible sensor made of a MCNP layer casted on a flexible substrate can be describe as the slope of the relative resistance ($\Delta R/R_b$, where R_b is the baseline resistance with no load applied on the sensor, and ΔR is the resistance change between R_b and the resistance when load is applied on the sensor). This response versus the load is the sensor's ***load sensitivity***. Since the deflection of the flexible sensors is directly proportional to the response of the sensor, the relation between the sensor's sensitivity, load, and the substrate parameters is given by

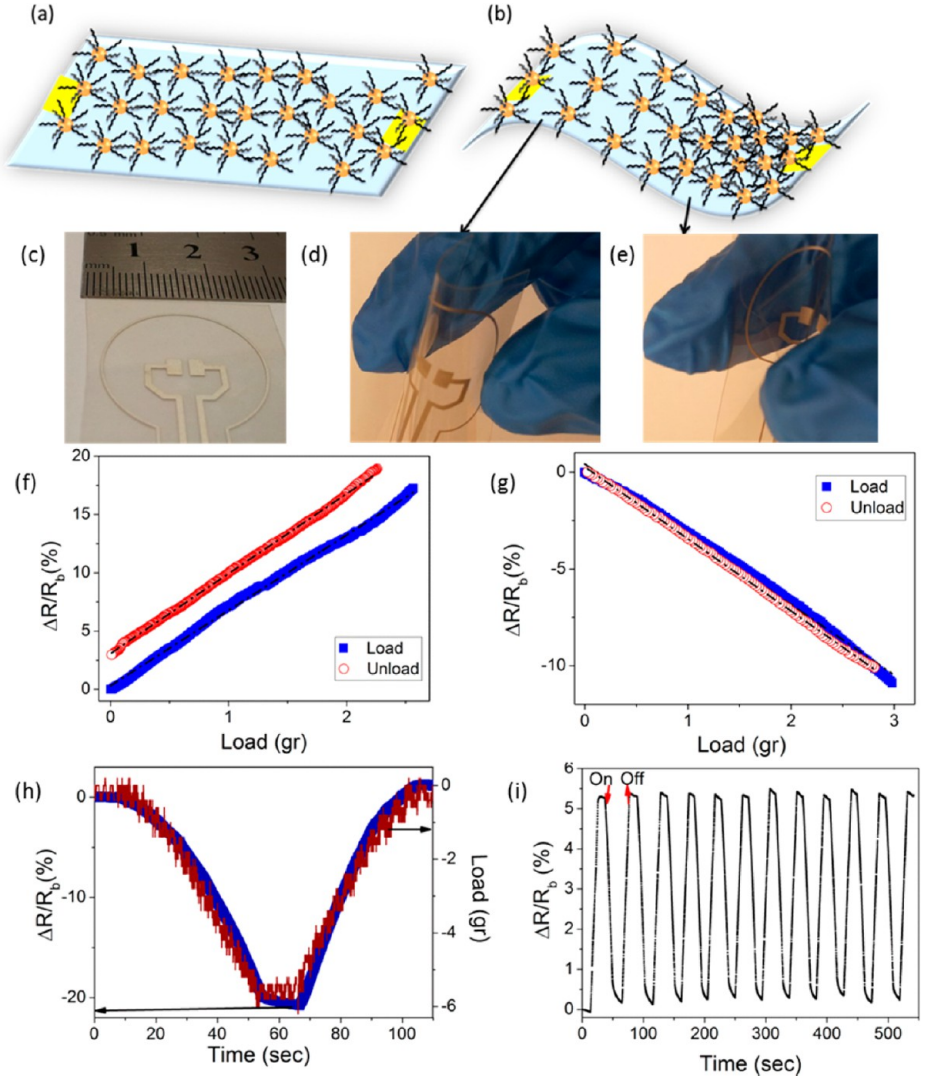

Figure 2. Schematic illustration of (a) the relaxed substrate with ETP-MCNPs film and (b) the bent substrate with ETP-MCNPs film and the effect of the bending on the ETP-MCNPs spacing. (c–e): Photographs of the actual device on PET in (c) relaxed state, (d) upward bent, and (e) downward bent. The distance between the electrodes is 1 mm. Relative response of the ETP-MCNP-based sensor to the PET's (f) stretch and (g) compression, by stress loading and unloading during three-point bending measurements. The black dashed lines are a linear fit to the curves, with R^2 in the range of 0.996–0.999 for all 4 curves. The sensitivity limit is down to tens of Pa, with 40 Pa being the limit of detection for this specific substrate. (h) Relative response of the ETP-MCNP sensor (thick blue line) for load/unload actions (thin red line) vs time. (i) Repeatability of sensor's response to load of 0.75 g.

$$\frac{\frac{\Delta R}{R_b}}{\Delta P} \propto \frac{1}{EI} \tag{3}$$

where ΔP is the load change. **It should be noted** that all the load units in this study are presented in "grams", for intuitive understanding of the discussed loads (1 g ≈ 0.01 N).

In the stretching setup, the strain/force was applied between two metal grips on a dog bone sample that is illustrated in Figure 1b. A MARK 10 ESM301 motorized test stand was used to apply strain in a constant speed of 1.5 mm/sec between metal grips that were attached to the wider part of the sample, while most of the strain occurs in the thinner part of the sample. The forces were measured by Advanced Digital FORCE GAUGE, made by Mark10 USA. Generally speaking, stretching a sample, while applying forces in the substrate's linear elastic regime of the stress–strain curve, follows Hooke's law:

$$\sigma = \varepsilon E \tag{4}$$

where σ is the applied force divided by the cross sectional area (the substrates thickness, h, multiplied by its width), ε is the strain in sample and E is the Young's modulus. In this setup, the width of all the sensors was equal. Therefore, the load sensitivity is expressed by

$$\frac{\frac{\Delta R}{R_b}}{\Delta P} \propto \frac{1}{Eh} \tag{5}$$

where h is the substrate thickness. Note that for stretching, specific load sensitivity will require much higher forces than in a bending setup. This is a consequence of the difference between equations for bending setup were the load is proportional to h^3 and equations for stretching setup were the load is proportional to h.

Evaluation of Temperature and Relative Humidity Sensing. Sensors were mounted on a custom polytetrafluoroethylene (PTFE) circuit board. The board was mounted inside a stainless steel test chamber with a volume of less than 300 cm^3. Controlled relative humidity levels (5–60% RH), purified dry nitrogen (99.9999%) from a commercial nitrogen generator (N-30, On Site Gas Systems, USA) equipped with a nitrogen purifier was used as carrier gas. The dry nitrogen was mixed with humidified air generated by the system's humidifier module. Controlled temperatures were produced by a

dx.doi.org/10.1021/am400757q | ACS Appl. Mater. Interfaces 2013, 5, 5531–5541

custom-made temperature controller. The sensing experiments were carried out by monitoring the response of the MCNP-based sensors to different relative humidity and temperature levels generated by the system, with and without applied force on the tested sensors. A Keithley data-logger device (model 2701 DMM) controlled by a custom Labview program was used to sequentially acquire resistance readings from the sensor array and voltage readings from the environmental sensors.

Preparation of the Integrated Pressure/Temperature/Humidity Sensors. Humidity or temperature sensors based on MCNP layers on SiO_2 substrate were prepared by drop casting aliquots of MCNP solution on interdigitated electrodes consisting of 24 pairs of Au electrodes (5 μm width and 25 μm spacing between adjacent electrodes) on a silicon wafer with a 1000 nm SiO_2 film. Between those sensors, a flexible ETP-MCNP layer on PET substrate was placed. The electrodes on the PET were mash printed by CPC Hi Technologies Ltd. with spacing of 1 mm.

RESULTS

Effect of Bending on the Flexible MCNP Sensors. Pressure sensors made of gold nanoparticles with 3-ethoxythiophenol as capping ligand (herewith, ETP-MCNP) on flexible polyethylene terephthalate (PET) substrates were examined by a three-point bending test (see Experimental), under bending and stretching conditions.[54] All experiments were carried out while maintaining the room temperature at 20 ± 1 °C and the relative humidity (RH) level at 50 ± 3%.

Figure 2 presents load and unload curves of the ETP-MCNPs strain sensor on PET substrate. Figures 2a and 2b are schematic illustration of the MCNP on relaxed and bent substrate. Figures 2c−e are optic images of the relaxed and bent PET substrate with printed electrodes. As seen in the figure, the relative resistance responses ($\Delta R/R_b$) were obtained when the ETP-MCNP films were stretched in one case and compressed in the other case. The positive or negative changes in resistance were linear upon gradual change of the bending level of the PET substrate. Indeed, placing the ETP-MCNP film on the PET's top side and bending the substrate compresses the ETP-MCNP film, bringing the ETP-MCNPs closer together, allowing higher tunneling currents, and, therefore, decreasing the measured resistance (see Figure 2e and 2g). When the ETP-MCNPs film is placed on the PET's bottom side, bending the substrate increases the distance between the adjacent ETP-MCNPs, resulting in a smaller tunneling current and, therefore, increasing the measured resistance (see Figure 2d and 2f). Figure 2h shows the ETP-MCNP sensor's responses upon continuous compression load and unload (thin red line) and the changing load (thick blue line) with time. As can be seen, the sensor's response closely follows the load curve. The maximum load was about 6 g and the corresponding response was ∼20%. In addition, the baseline resistance of the sensor after the load-unload cycle was similar. Figure 2i shows the high repeatability of the response of the ETP-MCNP sensor to stretching when subjected to 12 cycles of load (0.75 g) and unload. The load and unload were obtained by applying constant strain speed of 5 mm/min. As could be seen in the figure, the change in the relative resistance response to the load was about 5%. The sensor's response was repeatable with 1.5% relative standard deviation of the response (5% ± 0.075%), and with ∼2% relative standard deviation of baseline resistance values. Similar results were obtained using gold nanoparticles capped with decanethiol (*herewith*, DT-MCNP) on flexible polyethylene (PE) substrate (see Supporting Information, section 1). To test the feasibility of the studied devices for low-power electronic application, some bending experiments were carried out upon supplying a voltage of 0.5 V. The MCNP sensor responses showed similar results to those obtained at higher voltages (up to 5 V).

The Substrate Effect on the Morphology and the Load Sensitivity of the MCNP Films. In this study, the sensors' relative response ($\Delta R/R_b$) was proportional to the deflection (for the bending setup). Since high deflection can cause irreversible changes both in the flexible substrate and in the MCNP layer, a range of load sensitivities is required. This way, high loads will be measurable using thick substrates with high Young's modulus and small loads will be measured using thin substrates with small Young's modulus.

The relation between the substrate properties and the MCNP-based load sensors was explored by deposition of ETP-MCNP films on (i) substrates having similar composition (e.g., the same polymer like Kapton) but different thicknesses (50−130 μm) and (ii) substrates that had different compositions (e.g., different polymers) but similar thicknesses (e.g., 50 μm thick substrates of Kapton and Mylar). The names and properties of the flexible substrates are listed in Table 1.

The surface morphology of ETP-MCNP films on different substrates was studied by field emission high-resolution scanning electron microscopy (FE-HRSEM) and atomic force microscopy (AFM). Figure 3 presents the characterization of

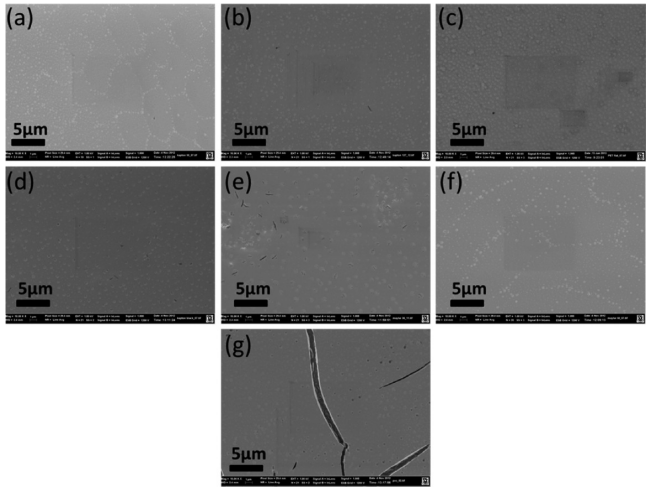

Figure 3. FE-HRSEM images of ETP-MCNP drop-casted layer on (a) Kapton 50, (b) Kapton 127, (c) PET 125, (d) Kapton b131, (e) Mylar 36, (f) Mylar 50, and (g) PVC 200, using SE detector, see Supporting Information, Figures S3−S6 for FE-HRSEM at different magnifications and additional areas in the MCNP film.

the center of the deposited ETP-MCNP drop on the various substrates studied here (cf. Table 1). Excluding PVC 200, all substrates exhibited highly continuous films, with different substrates leading to different density of "bubbles". For PVC 200, cracks appeared all over the layer. Nevertheless, continuous surface areas were observed between the cracks (Figure 3g). The layer thickness varied between 400 and 900 nm over the center of the drop (as estimated by AFM measurements). Detailed investigation and FE-HRSEM images (at different magnification levels) of the ETP-MCNP film can be found in the Supporting Information, section 2 and Figures S3−S6 therein.

Figure 4 shows the response of the pressure sensors as measured by 3-point bending tests. All experiments were

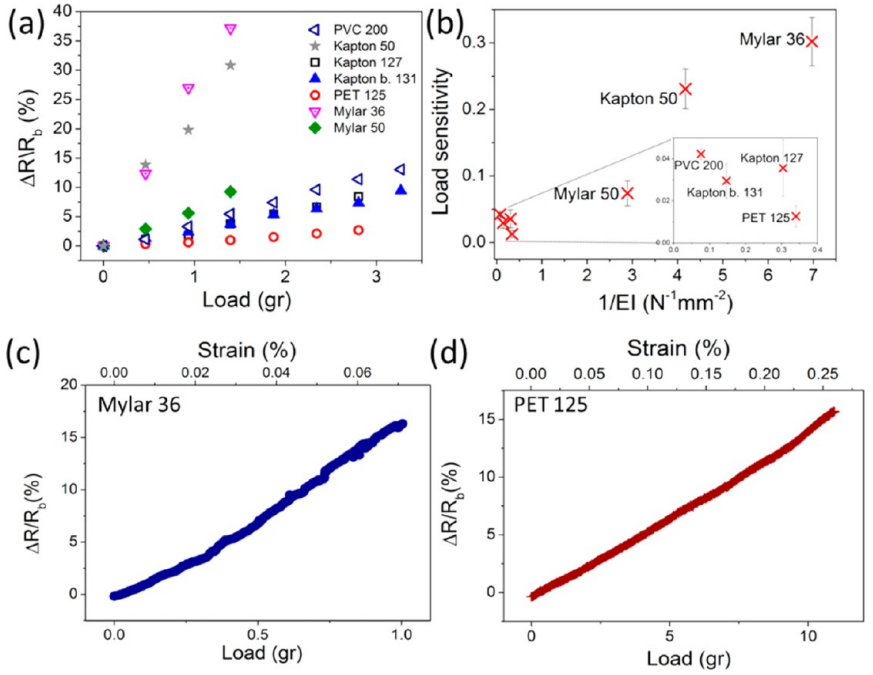

Figure 4. (a) Relative response ($\Delta R/R_b$) of ETP-MCNP films on different flexible substrates versus load, as measured by three-point bending tests. All the sensors were subjected to a series of loads. The response increases linearly with increasing load. The slope is a measure for the load sensitivity and depends on the substrates' mechanical and geometrical properties. The average responses presented are the average of 3−5 separate sensors. (b) The load sensitivity of the sensors having substrates with different properties, as function of the Young's modulus, geometrical property, and moment of inertia. The results show clear dependence of the sensors sensitivity on the substrate's properties. (c−d) $\Delta R/R_b$ versus load (bottom *x*-axis) and strain (upper *x*-axis) for (d) ETP-MCNP film deposited on Mylar 36 (load sensitivity = 0.31) subjected to loads that range between 200 mg to 1 g (d) ETP-MCNP film deposited on PET 125 (load sensitivity = 0.01) subjected to loads that range between 200 mg to 10 g.

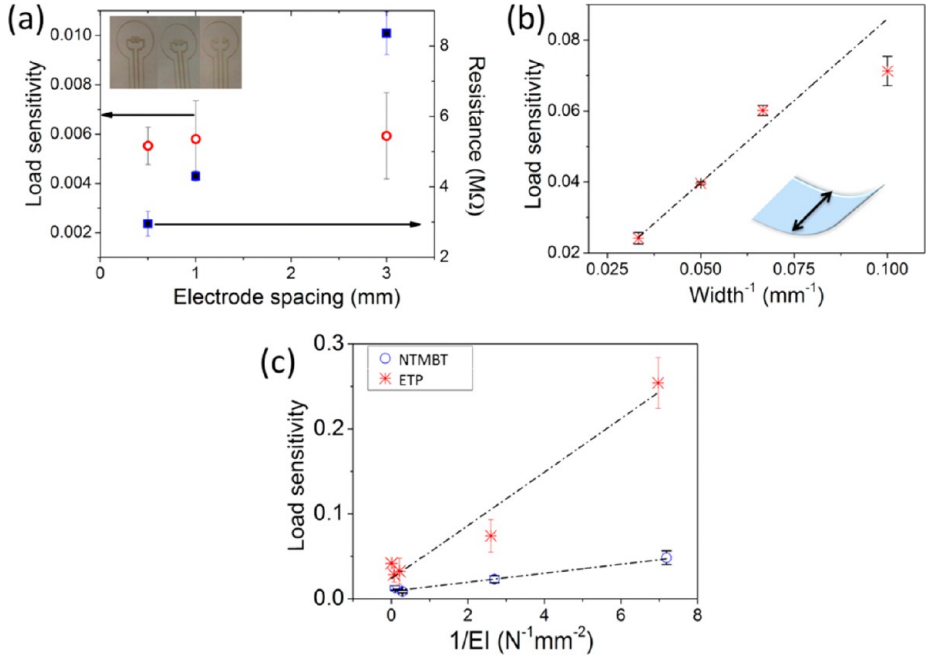

Figure 5. (a) The change in the load sensitivity (left *Y*-axis) and sensors' resistance (right *Y*-axis) for sensors fabricated on electrodes with 0.5, 1, and 3 mm spacing. The error bars are the standard deviation of three tested sensors for specific electrode spacing. (b) The change in load sensitivity for the same electrode structure and substrate with changing width of the substrate. The error bars are the standard deviation of 3 repetitions of the same sensor with specific dimensions. (c) The change in load sensitivity for different MCNP ligands. The black dashed lines are linear fits to the curves and the error bars are standard deviation of three sensors.

performed while maintaining the room temperature at 20 ± 1 °C and the RH level at 50 ± 3%. The electrical measurements were carried out using silver electrodes with 1 mm spacing between them. The sensors were tested under a series of loads (0.5−3.5 g) and the average responses ($\Delta R/R_b$) were calculated from 3 to 5 duplicates (Figure 4a). As could be

dx.doi.org/10.1021/am400757q | ACS Appl. Mater. Interfaces 2013, 5, 5531−5541

seen in the figure, applying a specific load on different substrates that are coated with similar ETP-MCNP layers exhibited noticeable differences in the response. For example, applying a load that is equal to 0.9 g on Kapton b. 131 coated with an ETP-MCNP film yielded a lower response (~3%) than for Mylar 36 coated with a similar ETP-MCNP film (~27%). This difference could be attributed to the larger elasticity of Mylar 36 substrate, which lead to greater separation between the ETP-MCNPs of the sensing layer (when the ETP-MCNPs film is on the bottom side of the substrate).[52] Figure 4b shows the average load sensitivities of the examined substrates as a function of the inverse of the product of the substrates' Young's modulus and the moment of inertia. As seen in the figure, the load sensitivity clearly depends on the substrate properties. More specifically, there is a positive trend where thinner substrates with smaller Young's modulus have higher load sensitivity. The error bars in Figure 4b represent the standard deviation of 3−5 similar substrates with electrodes. For most substrates, the standard deviation was smaller by an order of magnitude than the load sensitivity mean value. Similar results were obtained for the stretching setup (see Supporting Information, section 1 and Figure S2). In this case, the response of ETP-MCNP sensors followed closely the load curve (see Supporting Information, Figure S2a) and a positive linear trend for the load sensitivity as a function of the substrates' properties was measured (see Supporting Information, Figure S2b).

To estimate the range of the load sensitivities, two types of sensors were examined under various loads: (i) an ETP-MCNP film deposited on Mylar 36 (load sensitivity = 0.31) was subjected to 200 mg−1 g loads and (ii) an ETP-MCNP film deposited on PET 125 (load sensitivity = 0.01) was subjected to 200 mg−10 g loads. Figure 4c and d presents $\Delta R/R_b$ versus the load (bottom x-axis) and the strain (upper x-axis). As seen in the figure, changing the substrate's type would change the sensor's response to a specific load and strain. If a high response to low strains and loads is required, a sensor with high load sensitivity, like Mylar 36 (Figure 4c), can be chosen that has ~15% response to 1 gr load and to 0.07% strain. For higher strains and load range, a sensor with smaller load sensitivity would be suitable, like PET 125 (Figure 4d), which can sense up to 10 gr load and 0.25% strain.

Fine-Tuning the Load Sensitivity of the MCNP-based Flexible Sensors. For further understanding the controllability of the load sensitivity of the sensors, additional parameters were examined: (i) electrode spacing, (ii) substrate related parameters (e.g., width), and (iii) MCNP film related parameters (e.g., capping ligand), see Figure 5. To determine the electrodes' spacing effect, an ETP-MCNP layer was casted on different electrodes with spacing ranging from 0.5 to 3 mm. The results showed that the spacing between the electrodes has a negligible effect on the load sensitivity. In contrast, the spacing between the electrodes dramatically changed the baseline resistance. For example, ETP-MCNP film casted on electrodes spacing of 1 mm have a typical baseline resistance of 4 MΩ, while similar ETP-MCNP film casted on 3 mm electrodes spacing have a baseline resistance of 8 MΩ (Figure 5a). This result implies that the load sensitivity is independent of the baseline resistance. Images of the electrodes structure are presented in the inset of Figure 5a.

Figure 5b demonstrates a simple way to control the load sensitivity, using an ETP-MCNP layer casted on Kapton 127 having different substrate dimensions. By cutting the substrate width from 30 to 10 mm, the load sensitivity was improved by a factor of 3.5.

An additional way to control the sensitivity of the MCNP-based flexible sensors could come from the capping MCNP layer. Generally speaking, the MCNPs' organic ligands affect the chemical bonds and the bond strength between neighboring MCNPs and, therefore, might affect the load sensitivity. The tunneling decay constant determining the change in resistance is also different for different capping ligands. Figure 5c presents the change in load sensitivity upon replacing the capping ligand from ETP to nitro-4-trifluoro-methylbenzenethiol (herewith, NTMBT) and casting both MCNPs types on 5 different substrates (represented in the X-axis by their Young's modulus, E, and by their moment of inertia, I). As can be seen in the figure, the trend of the load sensitivity as a function of the substrate properties was positive for both ETP-MCNP and NTMBT-MCNP films. Nevertheless, all NTMBT-MCNP sensors exhibited lower load sensitivities.

Flexible MCNP Sensors as Strain Gauges. Figure 6 present the Gauge Factor (GF) of ETP-MCNP sensors (blue asterisks). GF is a measure that characterizes the sensitivity of the sensors as strain gauge, namely, the ratio between $\Delta R/R_b$ and ε. The GF is the slope of the linear fit of the sensors' relative response curves as a function of the strain. In the bending setup, the strain is proportional to the substrate thickness; therefore, the GF will be proportional to the inverse of the thickness. As can be seen in Figure 6, there is a linear trend between the GF and the inverse of the thickness. Of special interest, a GF = 250 could be achieved with ETP-MCNP films deposited on thin substrates (36 μm). So far, this GF value is at least two times higher than the previously reported MCNP-based strain gauges[11,35−37] (red circles in Figure 6): see Table 2 for more details on this comparison.

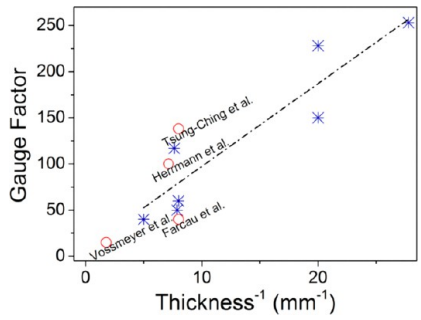

Figure 6. Gauge factor (GF) values that were extracted from linear fits of the sensors relative response vs the strain. The blue asterisks are the results of this work and the red circles are GF from previously reported MCNP-based sensors, reported by Farcau et al.,[37] Herrmann et al.,[11] Tsung-Ching et al.[35], and Vossmeyer et al.[25] The dashed black line is a linear fit.

Fatigue Properties of Flexible MCNP Sensors. The fatigue properties over a large number of bending cycles were tested using three sensors with Kapton 127 as flexible substrate and ETP-MCNP as the sensing layer. Those sensors were submitted to a strain of 0.3% for **10,000 cycles**. For one of the sensors the baseline resistances changed dramatically and, therefore, this sensor is not presented. For the other two sensors (S1 and S2), the baseline resistance showed a drift upon increasing the number of the bending cycles (see Figure 7a and 7b). The maximum drift in the baseline resistance was ~9%. While part of the drift could be attributed to the sensor

Table 2. Gauge Sensors Reported in the Literature

nanoparticle diameter (nm)	GF	substrate	ref
14	35−41	PET[a] 125 μm	Farcau et al.[37]
18	135	PET[a] 125 μm	Tsung-Ching et al.[35]
4	10−20	LDPE[b] 560 μm	Vossmeyer et al.[25]
18	100	photoresist 140 μm	Herrmann et al.[11]
2−5	50−250 (substrate depended)	variety of substrates	Present work

[a]PET = Polyethylene terephthalate. [b]LDPE = Low-density polyethylene.

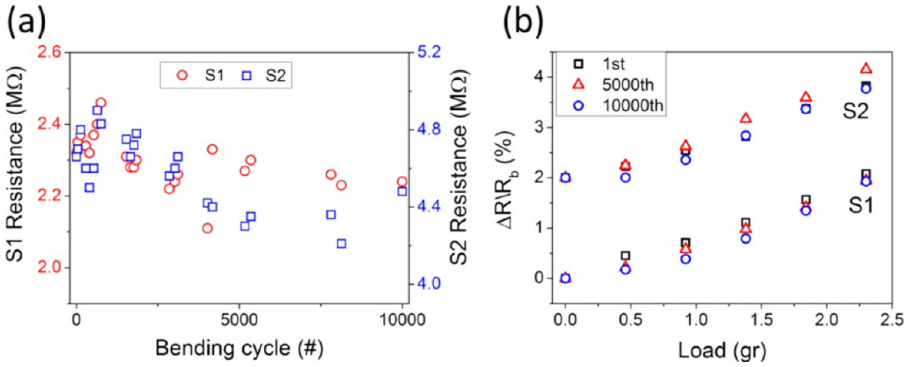

Figure 7. (a) Change in the baseline of ETP-MCNP/Kapton-127 sensors. (b) $\Delta R/R_b$ versus load after 1, 5000, and 10000 bending cycles.

per se, another part of the drift could be attributed to changes in the temperature and RH during the measurement. In contrast to the baseline behavior, the $\Delta R/R_b$ changed only slightly (2%) after 10,000 bending cycles.

Integrated Measurement of Pressure, Temperature and Humidity. Sensing various parameters (e.g., pressure, temperature, humidity) from a complex sample using a single chemistry of MCNPs would be an essential step toward imitating the multiparametric performance of the living skin.

For a proof-of-concept, a prototype based on MCNP technology was prepared and its abilities to measure the surrounding temperature, RH and applied load were estimated. Different (rigid) substrates were used to eliminate the load sensing from part of the sensors, and different capping ligands were chosen to isolate the sensing of RH or temperature. Two sensors were fabricated by casting ETP-MCNP and NTMBT-MCNP on silicon oxide with evaporated interdigitated gold electrode (see Experimental Section). A third sensor was fabricated by casting ETP-MCNPs on a PET substrate with 1 mm electrodes spacing (see Figure 8). The rigid sensors were taped on the flexible PET to form a single unit.

Figure 8. Schematic illustration of a prototype that is able to sense temperature, RH and load using different substrates (PET substrate in the center and silicon oxide substrates in sides) and 2 different MCNPs. The gold lines represent the metal electrodes.

Temperature and humidity were determined using the inflexible sensors. For sensing RH, a perforated NTMBT-MCNP film was used, as was described elsewhere.[30] This sensor has a large negative response (up to 80%) to increasing levels of RH due to ionization mechanism.[30] To sense mainly temperature changes, a highly concentrated ETP-MCNP solution (50 mg/mL) was casted on a silicon oxide substrate, resulting in a film with 500 nm thickness (estimated by AFM). The film's thickness was higher than the thickness of the evaporated gold electrodes (350 nm). It is therefore possible that the active swelled layer is not measured.[55] The responses of the inflexible sensors upon exposure to temperature and RH are presented in the Supporting Information, section 3 and Figure S7 therein.

The prototype was exposed to different temperature and RH cycles controlled by the air conditioning in the room. The RH range was 33−60% and the temperature range was 15−22 °C. The average errors from the values measured by external sensors of 6 different cycles are summarized in the Supporting Information, Table S1. When averaging all cycles, the temperature average error was 4.8 ± 1.4% and the RH average error was 9.3 ± 7%.

The possibility to integrate temperature and RH sensing capabilities within the MCNP-based touch platforms was examined using an ETP-MCNP sensor on a PET substrate. The first step was the examination of the sensor's responses to temperature and RH. For this purpose, the sensor was placed in a vacuum chamber with a controllable environment. The temperature and the RH were altered separately, and the corresponding $\Delta R/R_b$ was monitored. Figure S8 of the Supporting Information shows that the $\Delta R/R_b$ decreased exponentially with the temperature and that the increase in the sensing signal can be approximated as linear to the measured RH levels, with a sensitivity that is down to a single percent RH.

Next, an unknown load applied on the flexible ETP-MCNP sensor was estimated. For this purpose an algorithm that accounts for the temperature, RH and load was applied. In general, the change in resistance of a given sensor is caused by the change in these three values: temperature, RH and load. The effect of each parameter may be either linear or nonlinear. Either way, modeling and predicting a sensor's resistance due to changes in RH and temperature under a given load would still be achievable. To demonstrate the ability to easily model the effect of RH and temperature, several experiments were carried

out. The understanding of how temperature and RH affect this flexible sensor was established by exposing the sensor to a range of temperatures (23−38 °C) at two different constant RH conditions and exposing the sensor to a range of RHs (22−63%) at three constant temperatures. Figure 9a shows the

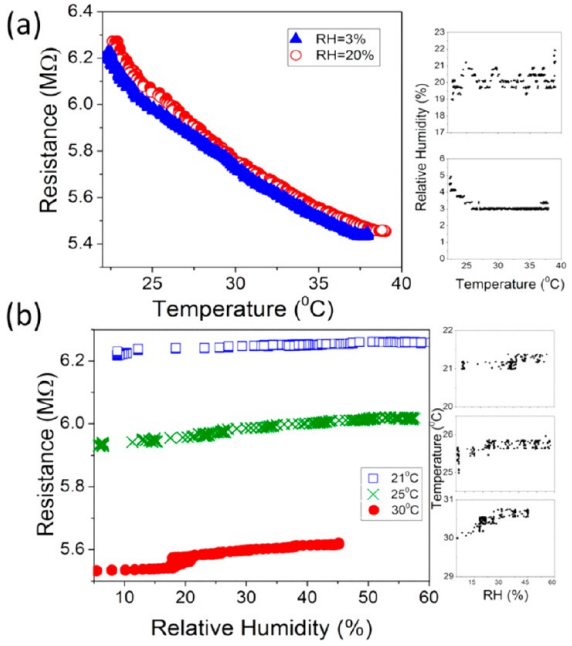

Figure 9. (a) Resistance of flexible ETP-MCNP sensor on PET substrate as a function of the temperature at 3% RH (blue full triangles) and at 20% RH (red hollow circles). The plots on the right describe the RH conditions during the temperature changing. (b) Resistance of flexible ETP-MCNP sensor on PET substrate as a function of % RH at 21 °C (blue hollow rectangle), 25 °C (green X), and 30 °C (red full circles). The plots on the right describe the temperature conditions during the RH variation.

resistance of the sensors versus the change in the temperature (it was found that there is an Arrhenius dependence of the logarithmic response as a function of $1/T$, not presented). The lines of the 2 different RH conditions were parallel to each the other. For small temperature ranges (~5 °C), the sensor's temperature dependence can be approximated as linear. Figure 9b also exhibits mostly linear and parallel responses upon increasing RH levels (beside a jump in 20% RH at 30 °C). Since it was not possible to keep constant condition for RH >25% when changing the temperature we assumed that this behavior represents the tested range. The dependence of the ETP-MCNP sensor's response on temperature (T) and relative humidity (RH) can be described in approximation as

$$R = R_{b0} + \Delta R_{RH}\cdot RH + \Delta R_T\cdot T \quad (6)$$

where R is the measured resistance of the sensor. ΔR_{RH} is the change in resistance per unity change in the RH. ΔR_T is the change in resistance per unity change in the temperature. R_{b0} is the extrapolated resistance under zero temperature and RH. A linear model was used to provide a simple proof of concept rather than a precise mathematical model. The linear equations provide a very good approximation as will be demonstrated further in the text. On the basis of this equation, the response of the flexible ETP-MCNP sensor can be described as a hyperplane in the "resistance vs temperature vs RH" space.

The three-sensor-based prototype was measured under changing environmental conditions as mentioned above. The flexible ETP-MCNP sensor was examined under different loads. The response of the flexible ETP-MCNP sensor to temperature (ΔR_T) and relative humidity (ΔR_{RH}) was different for various loads, and calculated using a solver script. The input parameters were the different environmental conditions (temperature and RH) and the corresponding resistance of the flexible ETP-MCNP sensor.

Figure 10 describes the different dependencies of the flexible ETP-MCNP sensor on temperature and on RH under zero

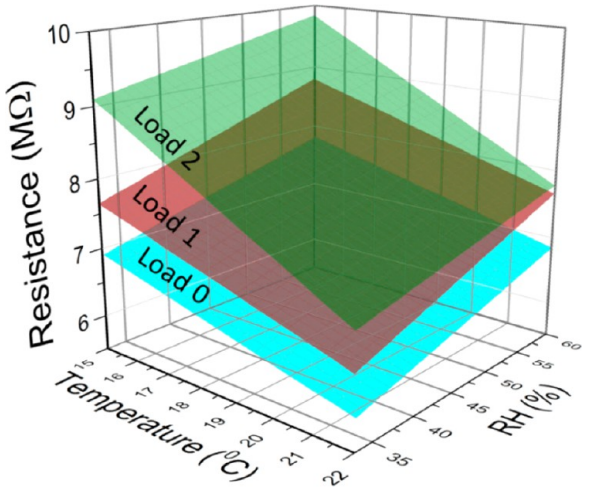

Figure 10. Calculated planes using eq 6 for an ETP-MCNP sensor on a PET substrate for 3 different loads. Load 0: Unloaded. Load 1: 3 g load. Load 2: 6 g load. The temperature and RH were measured by the inflexible ETP-MCNP and the NTMBT-MCNP sensors. The parameters from eq 6 were calculated using solver script.

load (Load 0), load of 3 g (Load 1), and a load of 6 g (Load 2). The temperature and RH were determined from the inflexible ETP-MCNP and NTMBT-MCNP sensors (see Figures 8 and Supporting Information, Figure S7). As can be seen in the Figure, the relative response to temperature and RH changed when different loads were applied (e.g., ΔR_{RH} and ΔR_T were dependent on the load).

The model's accuracy was estimated by measuring the load sensitivity of the ETP-MCNP sensor on PET substrate at specific temperatures and RHs, calculating the relative response of the sensor at those specific atmospheric conditions based on the planes that are presented in Figure 10, and calculating the applied force based on this data. The results are summarized in Table 3. As seen in this table, the model was able to estimate the load with less than 20% variance.

Table 3. Calculated and Real Loads Applied on an ETP-MCNP Sensor on a PET Substrate

	calculated load		
applied load (g)	18.7 °C, 47% RH (g)	19.7 °C, 45% RH (g)	21.4 °C, 43.5% RH (g)
3	2.42	2.8	3.07
6	6.7	6.68	6.08

dx.doi.org/10.1021/am400757q | ACS Appl. Mater. Interfaces 2013, 5, 5531−5541

DISCUSSION

Tuning of the Sensing Properties of Flexible MCNP-Based Sensors. A tunable load sensor based on an ETP-MCNP layer casted on a flexible substrate was presented. The relative responses to load were determined using a 3-point bending setup, where the MCNP layer is compressed or stretched (see Figure 2 and Supporting Information, Sections 1 and 2). For this bending setup, the perpendicular pressure is translated into measurable deformation in the flexible substrate and in the MCNP layer. The low standard deviations and the high signal-to-noise ratios of the signal's output for repeated load in Figure 2i ensure repeatable measurements of the sensors. When bending or stretching increases the distance between the nanoparticles (see Figure 2f; and Supporting Information, Section 1), there is an offset between the load and unload sensing curves. This offset can be attributed to irreversible changes in the ETP-MCNP layer like formation of cracks[56] or MCNP displacement. Despite this, the ETP-MCNP sensors exhibit excellent fatigue properties, so that the sensors' relative response changed only slightly (2%) after 10,000 bending cycles. Nevertheless, for applications of MCNP-based pressure/strain devices, further parameters that could contribute to this offset should be investigated (e.g., the contact between the electrodes and the MCNP layer).[57]

Highly continuous layers with different "bubble" densities were formed on all tested substrates (see Figure 3 and Supporting Information, Section 2), except on PVC 200. The layer margins or "coffee rings" were characterized as cracked areas that were probably not electrically conductive. Both the morphology of the coffee ring and the bubbles in the inner part of the layer can be explained by the capillary flow during the drying of the drops.[58−60] The difference in the bubble density might be attributed to the different adhesion between the ETP-MCNP solution and the different substrates, which, in turn leads to different capillary forces during the drying process of the drop. So far, it is not clear yet how those bubbles affect the sensing mechanism. On the other hand, the similar ETP-MCNP morphology on all examined substrates indicates that the main factor affecting the sensing parameters of the ETP-MCNP flexible sensors is the type of substrates per se.

There is a direct link between the substrate's properties and the measured load sensitivities, as described in eq 3, both in bending setup (Figure 4) and in stretching setup (Supporting Information, Section 1). The nonlinearity can be attributed to the different adhesion between the ETP-MCNP film and the various substrates. From Figure 4b and Figure S2b of the Supporting Information, it is evident that *the load sensitivity could be modulated by controlling the properties of the substrate, using the same MCNP ligands*. Hence, it could be possible to achieve a given sensing functionality without having to synthetize different MCNPs.

The tunability of the MCNP sensors was examined by exploring the influence of additional parameters (Figure 5). The results imply that the load sensitivity is independent of the baseline resistance. Adjusting the substrate's width can yield the required load sensitivities. This result emphasizes the ease of adjusting the load sensitivity. In addition, changing the capping ligand in the MCNP sensors also affects the load sensitivity. The same sensors can be used as highly sensitive strain gauges. Commercial strain gauges have typical gauge factor of 2. MCNP-based strain gauges have adjustable gauge factor that is dramatically affected by the substrate thickness (Figure 6). In this study a maximum gauge factor of 250 was achieved.

To demonstrate the utility of the finely tuned, MCNP-based flexible touch sensors, we have encoded letters using Morse code, namely, a combination of long and short pulses (lines and dots) that encode the whole alphabet and the 10 digits (see Figure 11a). Applying pressure with a finger to the surface of the sensor for short or long periods translated the pressure's magnitude and duration to pertinent electrical signals. Short responses in resistance were defined as dots and long responses were defined as a line (the pressure was roughly estimated as a single kPa). The sensing layer of ETP-MCNP was facing down during the pressing while there was no direct contact between the finger and the ETP-MCNP layer. In this way the effect of the finger's humidity and temperature on the sensing was minimized. Pressing on ETP-MCNP film that was deposited on **125 μm thick PET substrate** produced robust, precise and repeatable signals at the order of few percent (Figure 11b). Pressing on a similar ETP-MCNP film that was deposited on a different substrate, namely, **36 μm thick Mylar,** produced ×20−30 times higher responses (Figure 11c), thus implying the critical effect of the substrate's thickness on the sensor's responses. These results create an interesting possibility to fit the load sensitivity and range of touch sensors to a certain person. This way a highly sensitive sensor can be fitted, for example, to a small child's fingers, while another touch sensor can be fitted to the higher load sensing that are required for a grown person's fingers. Further tunability of the MCNP-based flexible Morse code device would be obtained by modifying the tunnel junctions and the interparticle gaps[34,36,49] by one or a combination of the following factors: the type of the capping monolayer,[49,56] the nanoparticle size (or diameter),[56,61] and/or the film's morphology.

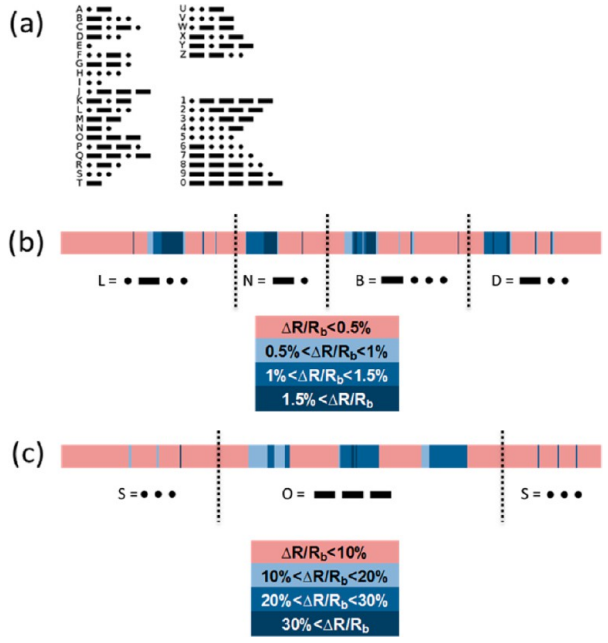

Figure 11. (a) Morse code table. (b) Encoding "SOS" on ETP-MCNP-based sensor with a 125 μm thick PET substrate. (c) Encoding "LNBD" on ETP-MCNP-based sensor with a 36 μm thick Mylar substrate. The pressure was applied using a finger (with an estimated pressure of approximately 1 kPa).

Simultaneous Measurement of Different Environmental Factors. Separation between the responses to pressure, temperature, and humidity of the MCNP-based sensors could be achieved by (i) the choice of the substrate; (ii) alternating the capping ligand or the deposition parameters, by, for example, layer-by-layer technique[62] or controlling the layer morphology, for example, perforated vs continuous morphology;[30] and (iii) using postmeasurement algorithmic compensation to extract or isolate the data affected by a single parameter (e.g., only temperature) as well as those affected by multiparametric sensors (temperature, humidity and strain).[23] The prototype that was presented in this study takes advantage of using different MCNP on inflexible substrate to sense temperature and humidity in an unconjugated manner. When a perforated MCNP film is formed, the main sensing mechanism for RH is condensation and ionization of water vapors on the exposed surface which generate negative responses of a high magnitude toward RH.[30] Without considering the difference of morphology, the sensing of temperature can be achieved by using a dense thick layer of ETP-MCNP on an inflexible substrate. This layer was thicker than the electrodes it was casted on. Therefore, exposure to RH cause changes in an unsensed part of the film. On the other hand, when temperature was altered, the properties of the whole film were sensitive to the change. In this way, the ETP-MCNP sensor was sensitive mainly to temperature (see Supporting Information, section 3).

A post measurement algorithm was used for the flexible ETP-MCNP sensor in order to isolate load sensing from sensing temperature and RH (Figures 9 and 10). When load was applied, the enlarging distance between the nanoparticles changed the surface coverage and in addition changed the morphology. All those changes should affect the MCNP sensor response in general. A better understanding of the effect of load on the sensing of features like temperature and RH is required in order to produce a more precise model.

In general, the explorative "3 in 1" prototype demonstrates the feasibility of using a SINGLE (or similar) MCNP chemistry with various substrate structures/designs to achieve multiparametric sensing on the same platform, such as *temperature, RH, and load*. Ongoing studies currently aim to extend these explorative results to wider ranges of temperature, humidity and MCNP chemistries. The results will be published elsewhere.

SUMMARY AND CONCLUSIONS

The characteristics of the MCNP-based sensing platforms make them excellent candidates for use as touch sensors for sensing a wide range of pressures that could eventually be implemented into e-skin technology. A major advantage of these touch sensors is the large span of loads they can measure, due to the ability of depositing MCNP layers on different substrates with various mechanical and geometrical properties. The ability to tune the load sensitivity by simple means such as changing the width of the sensors' substrate makes this technology applicable in many fields. In addition, it is possible to control the gauge factor of MCNP-based sensor by adjusting the substrate thickness. This option allows adjusting the desired load sensitivity and gauge factor of the sensor using the same MCNPs. Another important advantage of the MCNP-based sensors is their repeatable response even after a large number of bending cycles. For a multisensor that can sense load and environmental features, such as temperature and RH, there is no need for a complex integration of completely independent devices (humidity, temperature, and touch sensors). MCNP layers are compatible with large area deposition techniques, such as spray coating,[63] making their production cheap and simple.

The excellent touch (or pressure), temperature and humidity sensitivities of the MCNP-based flexible sensors could be important for the development of advanced e-skin devices. Those e-skin devices would be useful for wide variety of applications, such as, but not confined for (i) providing users with prosthetics an ability to measure environmental parameters through sensing touch in the form of different pressure levels;[64,65] (ii) transforming physical phenomena, such as strain deformation, into a measurable electrical signals in intelligent and communicative textile;[66] (iii) tracking the loads that soldiers have to carry and the effect of such loads on the soldier's physical response, which can be translated as the body temperature and humidity; and (iv) providing warnings about excess temperature and early formation of cracks in engines of cars and airplanes. Studies to demonstrate part of these applications as well as the morphology effect of the MCNP layers are currently ongoing in our laboratories and will be published elsewhere.

ASSOCIATED CONTENT

Supporting Information

Pressure sensor based on MCNPs (DT as encapsulating ligand and stretching setup for ETP-MCNP), characterization of the ETP-MCNP films by FE-HRSEM, and sensing temperature and relative humidity. This material is available free of charge via the Internet at http://pubs.acs.org.

AUTHOR INFORMATION

Corresponding Author

*E-mail: hhossam@technion.ac.il.

Notes

The authors declare no competing financial interest.

ACKNOWLEDGMENTS

The research leading to these results has received funding from the FP7's ERC grant under DIAG-CANCER (grant agreement no. 256639). The authors acknowledge Dr. Ulrike (Mirjam) Tisch for reviewing the paper and for helpful comments. H.H. is a Knight of the Order of Academic Palms.

REFERENCES

(1) Tiwana, M. I.; Redmond, S. J.; Lovell, N. H. *Sens. Actuators, A* **2012**, *179*, 17−31.
(2) Rogers, J. A.; Huang, Y. *Proc. Natl. Acad. Sci.* **2009**, *106*, 10875−10876.
(3) Wu, J. M.; Chen, C. Y.; Zhang, Y.; Chen, K. H.; Yang, Y.; Hu, Y.; He, J. H.; Wang, Z. L. *ACS Nano* **2012**, *6*, 4369−4374.
(4) Xiao, X.; Yuan, L.; Zhong, J.; Ding, T.; Liu, Y.; Cai, Z.; Rong, Y.; Han, H.; Zhou1, J.; Wang, Z. L. *Adv. Mater.* **2011**, *23*, 5440−5444.
(5) Takei, K.; Takahashi, T.; Ho, J. C.; Ko, H.; Gillies, A. G.; Leu, P. W.; Fearing, R. S.; Javey, A. *Nat. Mater.* **2010**, *9*, 821−826.
(6) Yamada, T.; Hayamizu, Y.; Yamamoto, Y.; Yomogida, Y.; Izadi-Najafabadi, A.; Futaba, D. N.; Hata, K. *Nat. Nanotechnol.* **2011**, *6*, 296−301.
(7) Lipomi, D. J.; Vosgueritchian, M.; Tee, B. C.; Hellstrom, S. L.; Lee, J. A.; Fox, C. H.; Bao, Z. *Nat. Nanotechnol.* **2011**, *6*, 788−792.
(8) Thostenson, E. T.; Chou, T. W. *Adv. Mater.* **2006**, *18*, 2837−2841.
(9) Kang, I.; Schulz, M. J.; Kim, J. H.; Shanov, V.; Shi, D. *Smart Mater. Struct.* **2006**, *15*, 737−748.

(10) Siffalovic, P.; Chitu, L.; Vegso, K.; Majkova, E.; Jergel, M.; Weis, M.; Luby, S.; Capek, I.; Keckes, J.; Maier, G. A.; Satka, A.; Perlich, J.; Roth, S. V. *Nanotechnology* **2010**, *21*, 385702.
(11) Herrmann, J.; Muller, K. H.; Reda, T.; Baxter, G. R.; Raguse, B.; de Groot, G. J. J. B.; Chai, R.; Roberts, M.; Wieczorek, L. *Appl. Phys. Lett.* **2007**, *91*, 183105.
(12) Maheshwari, V.; Saraf, R. F. *Science* **2006**, *312*, 1501−1504.
(13) Pang, C.; Lee, G. Y.; Kim, T. I.; Kim, S. M.; Kim, H. N.; Ahn, S. H.; Suh, K. Y. *Nat. Mater.* **2012**, *11*, 795−801.
(14) Mannsfeld, S. C. B.; Tee, B. C. K.; Stoltenberg, R. M.; Chen, C. V. H. H.; Barman, S.; Muir, B. V. O.; Sokolov, A. N.; Reese, C.; Bao, Z. *Nat. Mater.* **2010**, *9*, 859−864.
(15) Matsuzaki, R.; Keating, T.; Todoroki, A.; Hiraoka, N. *Sens. Actuators, A* **2008**, *148*, 1−9.
(16) Cosseddu, P.; Milita, S.; Bonfiglio, A. *IEEE Elec. Dev. Lett.* **2012**, *33*, 113−115.
(17) Yu-Jen, H.; Zhang, J.; Kymissis, I. *IEEE Elec. Dev. Lett.* **2011**, *58*, 910−917.
(18) Someya, T.; Sekitani, T.; Iba, S.; Kato, Y.; Kawaguchi, H.; Sakurai, T. *Proc. Nat. Acad. Sci.* **2004**, *101*, 9966−9970.
(19) Bay, J. S. *Robot. Automat. Mag.* **1995**, *2*, 36−43.
(20) Shunfeng, C.; Kwok, T.; Thomas, L.; Pecht, M. *IEEE Sens. J.* **2012**, *10*, 856−862.
(21) Lopez-Higuera, J. M.; Rodriguez Cobo, L.; Quintela Incera, A.; Cobo, A. *J. Lightwave Technol.* **2011**, *29*, 587−608.
(22) Arregui, F. J.; Matias, I. R.; Cooper, K. L.; Claus, R. O. *IEEE Sens. J.* **2002**, *2*, 482−487.
(23) Konvalina, G.; Haick, H. *ACS Appl. Mater. Interf.* **2012**, *4*, 317−325.
(24) Wang, L.; Luo, J.; Schadt, M. J.; Zhong, C. J. *Langmuir* **2010**, *26*, 618−632.
(25) Tsung-Ching, H.; Kwang-Ting, C. *J. Disper. Sci. Technol* **2009**, *5*, 206−215.
(26) Wuelfing, W. P.; Murray, R. W. *J. Phys. Chem. B* **2002**, *106*, 3139−3145.
(27) Haick, H. *J. Phys. D* **2007**, *40*, 7173−7186.
(28) Tisch, U.; Haick, H. *MRS Bull.* **2010**, *35*, 797−803.
(29) Tisch, U.; Haick, H. *Rev. Chem. Eng.* **2010**, *26*, 171−179.
(30) Segev-Bar, M.; Shuster, G.; Haick, H. *J. Phys. Chem. C.* **2012**, *116*, 15361−15368.
(31) Shuster, G.; Baltianski, S.; Tsur, Y.; Haick, H. *J. Phys. Chem. Lett.* **2011**, *2*, 1912−1916.
(32) Dovgolevsky, E.; Konvalina, G.; Tisch, U.; Haick, H. *J. Phys. Chem. C.* **2010**, *114*, 14042−14049.
(33) Dovgolevsky, E.; Haick, H. *Small* **2008**, *4*, 2059−2066.
(34) Dovgolevsky, E.; Tisch, U.; Haick, H. *Small* **2009**, *5*, 1158−1161.
(35) Vossmeyer, T.; Stolte, C.; Ijeh, M.; Kornowski, A.; Weller, H. *Adv. Funct. Mater.* **2008**, *18*, 1611−1616.
(36) Farcau, C.; Moreira, H.; Viallet, B.; Grisolia, J.; Ciuculescu-Pradines, D.; Amiens, C.; Ressier, L. *J. Phys. Chem. C.* **2011**, *115*, 14494−14499.
(37) Farcau, C.; Sangeetha, N. M.; Moreira, H.; Viallet, B.; Grisolia, J.; Ciuculescu-Pradines, D.; Ressier, L. *ACS Nano* **2011**, *5*, 7137−7143.
(38) Wang, L.; Luo, J.; Yin, J.; Zhang, H.; Wu, J.; Shi, X.; Crew, E.; Xu, Z.; Rendeng, Q.; Lu, S. *J. Mater. Chem.* **2009**, *20*, 907−915.
(39) Peng, G.; Tisch, U.; Adams, O.; Hakim, M.; Shehada, N.; Broza, Y. Y.; Billan, S.; Abdah-Bortnyak, R.; Kuten, A.; Haick, H. *Nature Nanotechnol.* **2009**, *4*, 669−673.
(40) Xu, Z. Q.; Broza, Y. Y.; Ionsecu, R.; Tisch, U.; Ding, L.; Liu, H.; Song, Q.; Pan, Y. Y.; Xiong, F.; Gu, K. S.; Sun, G. P.; Chen, Z. D.; Leja, M.; Haick, H. *Br. J. Cancer* **2013**, *108*, 941−950.
(41) Peled, N.; Hakim, M.; Bunn, P. A., Jr; Miller, Y. E.; Kennedy, T. C.; Mattei, J.; Mitchell, J. D.; Hirsch, F. R.; Haick, H. *J. Thorac. Oncol.* **2012**, *7*, 1528−1533.
(42) Peled, N.; Ionescu, R.; Nol, P.; Barash, O.; McCollum, M.; VerCauteren, K.; Koslow, M.; Stahl, R.; Rhyan, J.; Haick, H. *Sens. Actuat. B* **2012**, *171*, 588−594.
(43) Barash, O.; Peled, N.; Tisch, U.; Bunn, P. A.; Hirsch, F. R.; Haick, H. *Nanomedicine (New York, NY, U. S.)* **2012**, *8*, 580−589.
(44) Marom, O.; Nakhoul, F.; Tisch, U.; Shiban, A.; Abassi, Z.; Haick, H. *Nanomedicine (London, U. K.)* **2012**, *7*, 639−650.
(45) Tisch, U.; Schlesinger, I.; Ionescu, R.; Nassar, M.; Axelrod, N.; Robertman, D.; Tessler, Y.; Azar, F.; Marmur, A.; Aharon-Peretz, J.; Haick, H. *Nanomedicine (London, U. K.)* **2013**, *8*, 43−56.
(46) Tisch, U.; Aluf, Y.; Ionescu, R.; Nakhleh, M.; Bassal, R.; Axelrod, N.; Robertman, D.; Tessler, Y.; Finberg, J. P. M.; Haick, H. *ACS Chem. Neurosci* **2011**, *3*, 161−166.
(47) Peng, G.; Hakim, M.; Broza, Y. Y.; Billan, S.; Abdah-Bortnyak, R.; Kuten, A.; Tisch, U.; Haick, H. *Br. J. Cancer* **2010**, *103*, 542−551.
(48) Barash, O.; Peled, N.; Hirsch, F. R.; Haick, H. *Small* **2009**, *5*, 2618−2624.
(49) Moreira, H.; Grisolia, J.; Sangeetha, N. M.; Decorde, N.; Farcau, C.; Viallet, B.; Chen, K.; Viau, G.; Ressier, L. *Nanotechnology* **2013**, *24*, 095701.
(50) Ye, C.; Li, M.; Xue, M.; Shen, W.; Cao, T.; Song, Y.; Jiang, L. *J. Mater. Chem.* **2011**, *21*, 5234−5237.
(51) Qian, X.; Park, H. S. *J. Mech. Phys. Sol.* **2010**, *58*, 330−345.
(52) Alvares, D.; Wieczorek, L.; Raguse, B.; Ladouceur, F.; Lovell, N. H. *Procedia Eng.* **2011**, *25*, 1349−1352.
(53) For humidity sensor based on MCNPs with silver electrodes, humidity might lead to Ag migration in the conductive adhesive electrodes.
(54) Young, W. C. *Roark's Formulas for Stress and Strain*, 6th ed.; McGraw-Hill: New York, 1989.
(55) Steinecker, W. H.; Rowe, M. P.; Zellers, E. T. *Anal. Chem.* **2007**, *79*, 4977−4986.
(56) Olichwer, N.; Leib, E. W.; Halfar, A. H.; Petrov, A.; Vossmeyer, T. *ACS Appl. Mater. Interf.* **2012**, *4*, 6151−6161.
(57) Gilbert, J. R.; Ananthasuresh, G. K.; Senturia, S. D. In *3D modeling of Contact Problems and Hysteresis in Coupled Electro-Mechanics*, Micro Electro Mechanical Systems, 1996, MEMS'96, Proceedings.'An Investigation of Micro Structures, Sensors, Actuators, Machines and Systems'. IEEE, The Ninth Annual International Workshop on, 1996; IEEE: Washington, DC, 1996; pp 127−132.
(58) Deegan, R. D.; Bakajin, O.; Dupont, T. F.; Huber, G.; Nagel, S. R.; Witten, T. A. *Nature* **1997**, *389*, 827−828.
(59) Deegan, R. D.; Bakajin, O.; Dupont, T. F.; Huber, G.; Nagel, S. R.; Witten, T. A. *Phys. Rev. E* **2000**, *62*, 756−765.
(60) Deegan, R. D. *Phys. Rev. E* **2000**, *6*, 475−485.
(61) Sangeetha, N. M.; Decorde, N.; Viallet, B.; Viau, G.; Ressier, L. *J. Phys. Chem. C.* **2013**, *117*, 1935−1940.
(62) Joseph, Y.; Peić, A.; Chen, X.; Michl, J.; Vossmeyer, T.; Yasuda, A. *J. Phys. Chem. C.* **2007**, *111*, 12855−12859.
(63) Maenosono, S.; Okubo, T.; Yamaguchi, Y. *J. Nanopart. Res.* **2003**, *5*, 5−15.
(64) Lee, M. H.; Nicholls, H. R. *Mechatronics* **1999**, *9*, 1−31.
(65) Farserotu, J.; Baborowski, J.; Decotignie, J. D.; Dallemagne, P.; Enz, C.; Sebelius, F.; Rosen, B.; Antfolk, C.; Lundborg, G.; Bjorkman, A.; Knieling, T.; Gulde, P. Smart Skin for Tactile Prosthetics. In *6th International Symposium on Medical Information and Communication Technology (ISMICT)*, 25−29 March 2012; IEEE: Washington, DC, 2012; pp 1−8.
(66) Cochrane, C.; Koncar, V.; Lewandowski, M.; Dufour, C. *Sensors* **2007**, *7*, 473−492.